Analysis of Swarm Data to Explore Plasma Parameters in the Auroral Region

Cassandra Mckenna, I. R. Mann

Undergraduate Thesis

Submitted in Partial Fulfillment of the Physics Undergraduate Program

April 2024

1 Abstract

Research on the Ionospheric resonating cavity (IAR) dates back 40 years with 10-20 years of theoretical underpinning and 20 years of observations. With new advances in the capabilities of all sky images and in-situ electromagnetic measurements, the Resonatating cavities affects, such as aurora modulation, can be contextualized through optical observations alongside quantitative electromagnetic measurements. Previous research has focused on the presence of the resonating cavity –whether that be optically or electromagnetically – rather than a quantative description of the plasma parameters in-situ. By synthesizing analytical models to give physical quantities with high resolution in-situ optical and electromagnetic data, we can understand how the properties of the aurora, such as conductivity, change through spatiotemporal evolution! Due to the data limited nature of space physics, sanity checks were a major contributor to the length of this undergraduate thesis project and detailed descriptions of the methods used to quantitatively describe the IAR are described.

2 Background

The modulation of magnetospheric Alfven waves are an important process that may determine the energy-response seen in the aurora. Alfven waves are ubiquitous is space plasmas and propagate energy along the environmental magnetic field lines[1]. It has been known since the 70's that reflections of Alfven waves hitting the ionosphere is controlled by an effective conductance. [2] This is due to the speed profile of Alfven waves changing from its source, the magnetosphere, to the ionosphere. The speed profile is related to an effective Alfvenic conductivity (how easily the waves can travel through a media is the meaning of conductivity in this context) of

$$\Sigma_A = \frac{c^2}{4\pi V_A}$$

where Σ_A is the conductance and V_A is the Alfven speed. The physical interpretation of conductivity in an Electromagnetic wave is how easily the wave can pass through a media. Additionally, this

speed change and conductivity can be thought the lens of density changes in the meso-scale auroral system.

The plasma densities in the ionosphere is quite high approximately $10^6 cm^{-3}$ whereas in the magnetosphere values are closer to $1 cm^{-3}$. The Alfven speed is given as

$$V_A = \frac{B}{(\mu_0 \rho)^{\frac{1}{2}}}$$

. it is important to note that B does also have a height dependence; however, since Alfven waves travel along lines of constant magnetic field, B will not change so $V_A \propto \frac{1}{\rho}$. Additionally another physical consequence of this $\nabla\rho$ is that there will form an effective reflectance coefficient since the downward going Alfven encounters a denser medium and will bounce off (like light reflecting off water). The reflectance of Alfven waves creates stratifications in the upper ionosphere (from 400km up to a few R_E) where Alfven waves create cavities. The stratifications have the potential to make resonsating cavities which modulate the aurora through the percentage of Alfven waves which transmit. These resonating cavities have frequencies of Alfven waves which are transmitted and reflected and a real world example of the frequency striations can be seen in figure 1b.

However this view is further complicated by the fact that when Alfven waves carry current (for more info look at landau dampening). [1] As the number of Alfven waves transmitted changes, the current also changes (ie: more transmitted waves=more current). This creates a feedback instability where Alfven waves are not only modulated by the density gradients but the frequency response of the resonating cavity. This feedback instability could have the consequence of inducing auroral activity is subject to study as the resonating signature of this cavity is measurable with in-situ measurements.

The benefits of invoking models, and specifically Lysak's 1991 model, is that it gives a first order estimate to the ionospheric, known as Pedersen, conductivity. [4] [5]Conductance is an important plasma parameter as its describes the current being passed into the ionosphere:

$$\Sigma = \frac{\vec{J}}{\vec{E}}$$

Additionally, the Alfven speed for a given time series can be found by utilizing the reflection ratio, which in practice, can be found by find the cross component ratio of $\vec{E}/\vec{B}$. [6]. The analysis to get to this model is quite rigourous so a major of the rest of the manuscript will focus on the details before diving into the analysis. Additionally, we also look at All-Sky Cameras to understand the physical location these Alfven waves within the structure of the auroral oval. Previous research has found the structure of the alfven waves in the aurora is very local and changes through time [7]. Additionally, Miles. et al. 2018 located discrete arcs and associated Alfven waves find plasma parameters using the model through spatial evolution (lump sum calculation) . [7] By synthesizing a model to give physical quantities, with high resolution in-situ optical and electromagnetic data, we can understand how the properties of the aurora such as conductivity change through spatiotemporal evolution!

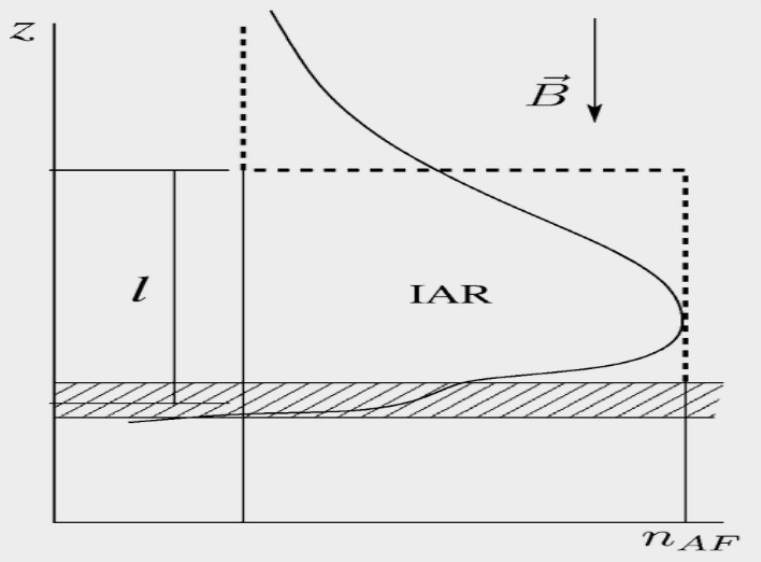

(a) Reflection index as a function of height in the Ionospheric Resonating Cavity Model, ℓ is the characteristic height

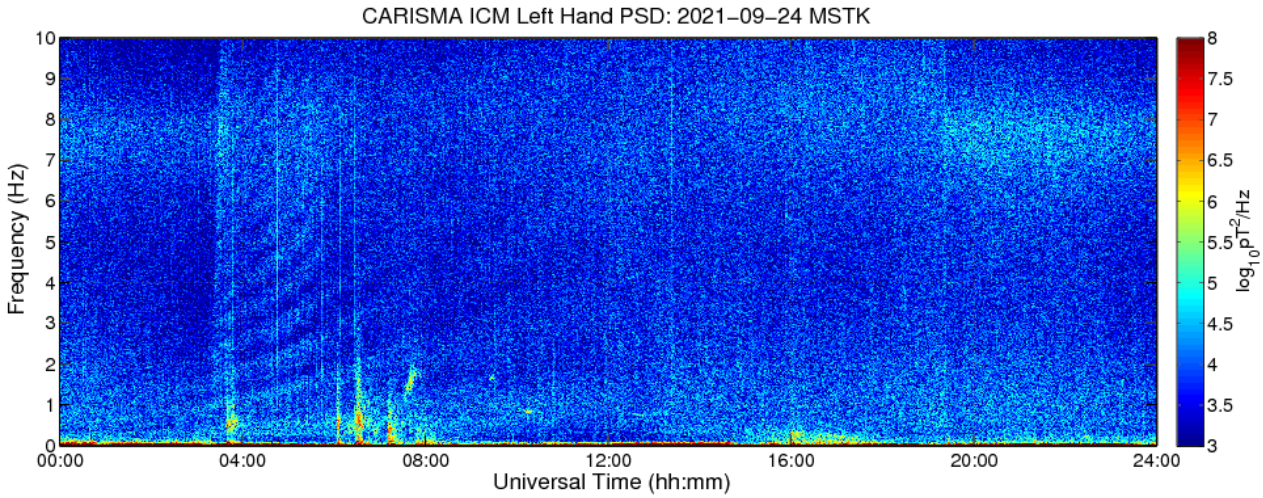

(b) Example of the Ionospheric resonator and its frequency signature as seen my the Carisma Magnetometer during the event studied in section 4 and 7[3]

Figure 1: Density Profile and its resulting Ionospheric Resonating Cavity as seen from ground based-magnometers

3 Model

3.1 Theory

Lysak's 1991 model [4], assumes that the effective conductivity of Alfven Waves changes exponentially from the ionosphere as

$$V_A = \frac{V_{AI}^2}{\epsilon^2 + e^{\frac{-z}{h}}}$$

Where V_A is the generalized Alfven speed, V_{AI} is the speed at the ionosphere, ϵ is the ratio of Alfven speed at the ionosphere over surface $\epsilon = \frac{V_{AI}}{V_{AM}}$, z is the height of the measurement (in our case the spacecraft) above the ionosphere, and h is a height integrated conductivity coefficient. Given the appropriate boundary condition we get a solution for the waves to be

$$\phi^{\pm} = J_{\pm ix_0\epsilon}(x)$$

where $x_0 \propto h, V_{AI}$ and $x = x_0 e^{-z/2h}$ and the subscript denotes the order of the Bessel function. In summary these waves are described the complex order and argument Bessel functions which depend on z, h, V_{AI} and the sign denotes the direction. Below in figure 2 is a model of the ratio of ϕ up and down

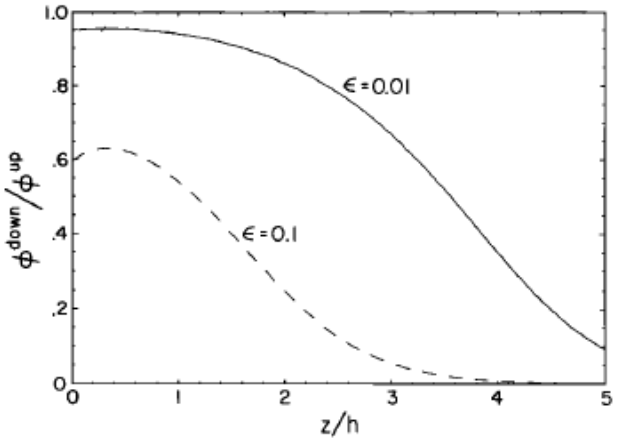

Figure 2: Ratio of down going Alfven waves versus upward going. Given the $\epsilon = 0.1$ we can see where the resonating cavity is located and how the transmissible of the plasma goes down. [4]

Moreover, the model denotes a reflection coefficient as the ratio of

$$R = \frac{iJ'_{ix_0\epsilon}(x_0) + \alpha J_{ix_0\epsilon}(x_0)}{iJ'_{-ix_0\epsilon}(x_0) + \alpha J_{-ix_0\epsilon}(x_0)}$$

where J' is the derivative of J and α is a coefficient of reflection. From Lysak, one consequence of the ionospheric resonating there will be interference in the electric and magnetic fields propagated from the Alfven waves. In practice this means that some frequencies are resonated in the cavity and do not reach the ionosphere. From this we can find experimental values for the conductivity of the ionosphere, the Alfven speed, height conductivity, and what frequencies are ommitted or transmitted by the resonating cavity.

3.2 Parameter testing

Lets go look at the phase space given by the solutions so we can better understand the model. On the x axis is the frequency and the y axis is the reflectance times the Alfven speed. By default the values are $\Sigma = 3S$, $V_{AI} = 300km/s$ and $h = 100km$

By looking at the zeroth order frequency, we find a first order approximation for the ionospheric conductivity Σ; however, at low conductivity, the zeroth order term is greater than the minima

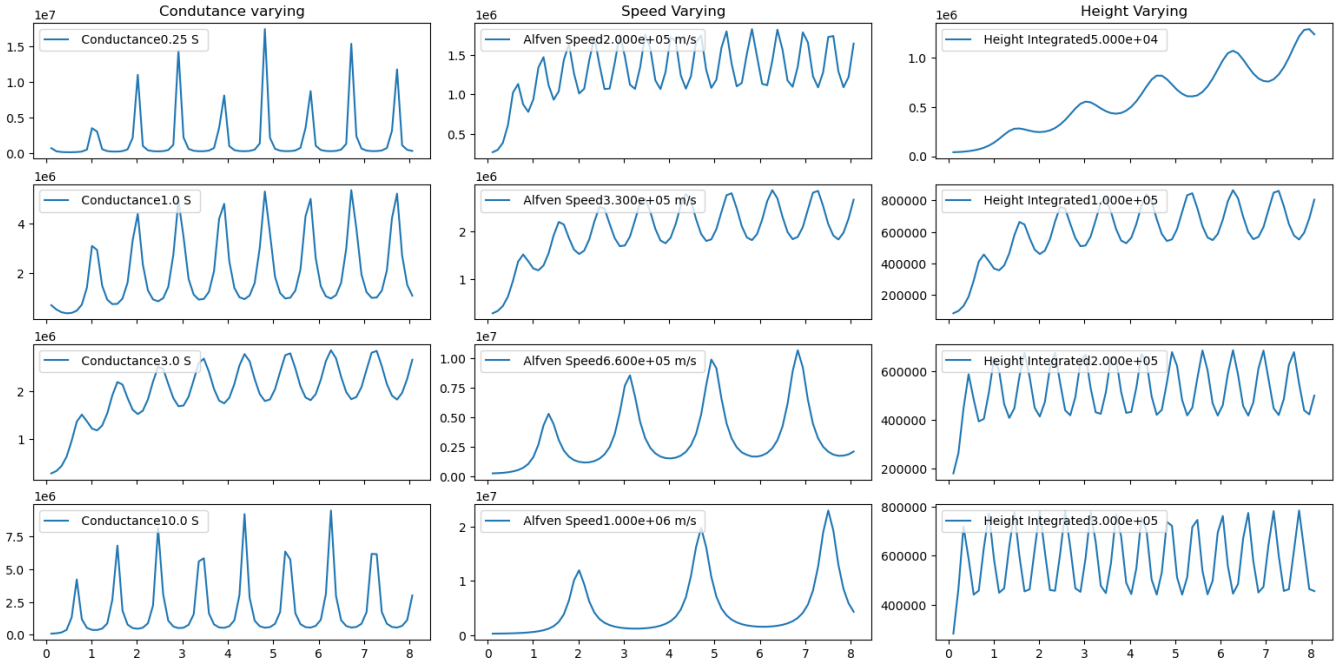

Figure 3: Varying parameters based on Lysak's Ionospheric Resonating cavity model. The Y axis is a-kin to the amplitude spectra seen in $\frac{E}{B}$ ratio.

observed between the zeroth frequency and next maxima. That means for our analysis later on in section 7 is only valid for conductivity where the zeroth frequency term is the smallest ampltiude term and the conductivity given is above 1. Note values of 0.25S to 10S are predicted by the The International Reference Ionosphere and work by Gjerloev et al. respectively. [8] [9]

Additionally, the behaviour of the Alfven speed with increasing values causes the frequency to decrease as well as an increase in amplitude. This agrees with the estimate of Alfven speed as the mean value of the wave should be the Alfven speed itself. Lastly the height integration reduces the amplitude and increases the frequency.

While all independent parameters, the resulting Bessel functions predicted by the model are extremely complicated and changes to the parameters creates large changes. To fit data to these models, intensive Monte Carlo are required which will be done at a future stage. I have done some tests of model versus model Bayesian Monte Carlo using pymc ; however, this was extremely intensive computationally and care is required on ensuring the in-situ measurements are up to the scrutiny of going through a Monte Carlo before proceeding. [10] The rest of this manuscript will focus on the sanity checking and scrutinizing the processing as well as the raw data of the in-situ electric and magnetic field measurements from Swarm.

4 Experimental setup

4.1 Swarm Satellites

The Swarm constellation consists of three space craft. One is in a high orbit of approximately 510km whereas the other two are together and are separated by a small longitudinal distance (0.1°) and are at

a height of $440km$. [11] Each satellite is equipped with a vector field magnetometer and an electric field instrument. The cadence of each is 50Hz and 16Hz. To access the quality of the Electric Field Instrument, raw thermal ion images are beamed down every 30 seconds which show the distribution of velocities. [12] [13] The density of velocities in these raw images can be used to infer the quality of the data. [14]. Additionally, automatic calibration and quality flags are associated with data points.

Both the electric and magnetic fields have background components that must be removed to see Alfven waves in the ionosphere. For the magnetic field data, its readings are given in the NEC coordinate system. Subtracting the mean field of the Earth's magnetic dynamo using the CHAOS model [15], we then get the magnetic field signal generated by the field aligned currents and Alfven modes. There is no background electric field in the ionosphere so no background removal is necessary; however, for both measurements we use a 20 second running average to calibrate the measurements further. This is done in order to visually see the ionospheric resonating cavity easier as the low-change plasma processes are reduced while the dynamic Alfven wave processes are more apparent.

Using the tools provided by University of Calgary's SwarmAurora and AuroraX, we found close conjunctions between Swarm space-craft with the Electric Field Instrument operating and the auroral all sky imagers at 03:46-03:48 September 2021.[16] As a discrete arc over Gilliam MB. appears and is conjunction with Swarm A and C satellites with their Electric and Magnetic field instruments running. Further analysis using the techniques described in chapter 3 is used to understand where Alfven waves are present in the auroral signature. The electric field instrument in Swarm C; however, is known to be of worse quality compared to Swarm B and C and the images of the histogram fit have artifacts unsuitable for analysis.[14] For this case we will use just the Swarm A data; however, the magnetic field data for Swarm C provides context to the electrodynamics of the pass through.

4.2 All Sky Cameras

4.2.1 Background

6 TREx-RGB cameras are located in 6 locations spanning the Canadian Aurora oval and mid latitudes. Skymaps, which provide latitude and longitude measurements for each value, are provided by the University of Calgary and allow for the collocation of satellites in the field of view of these all sky imagers. [17]

4.2.2 Mapping

Due to dipole nature of Earth's magnetic field, the position of the aurora and the electromagnetic measurements from the particle do not correspond to the same magnetic latitude and differing heights. Instead particles travel along the field lines which are curved. To correct for this we use IRBEM's some model to map down the field lines. [18] Validation is hard here so the baselines we know is that at the zenith, both the mapped and unmapped signatures should match since they are right overhead. [19] Additionally, due to the fish eye nature of the cameras, since the projection puts the space craft at the same speed but lower down, it will appear to traverse faster. Projected to a coordinate system which is aligned with latitude and longitude, these speed projections will disappear and instead the only observable affect will be an offset in position of the spacecraft (largely in latitude) from the dipole fields. Below is an example of a imager frame with and without mapping which corresponds to approximately. A whole summer project can be dedicated to the precise tomography of the mapping

to the auroral signature so for the effective of this manuscript a simple mapping with assumed auroral altitude of 110km is sufficient.

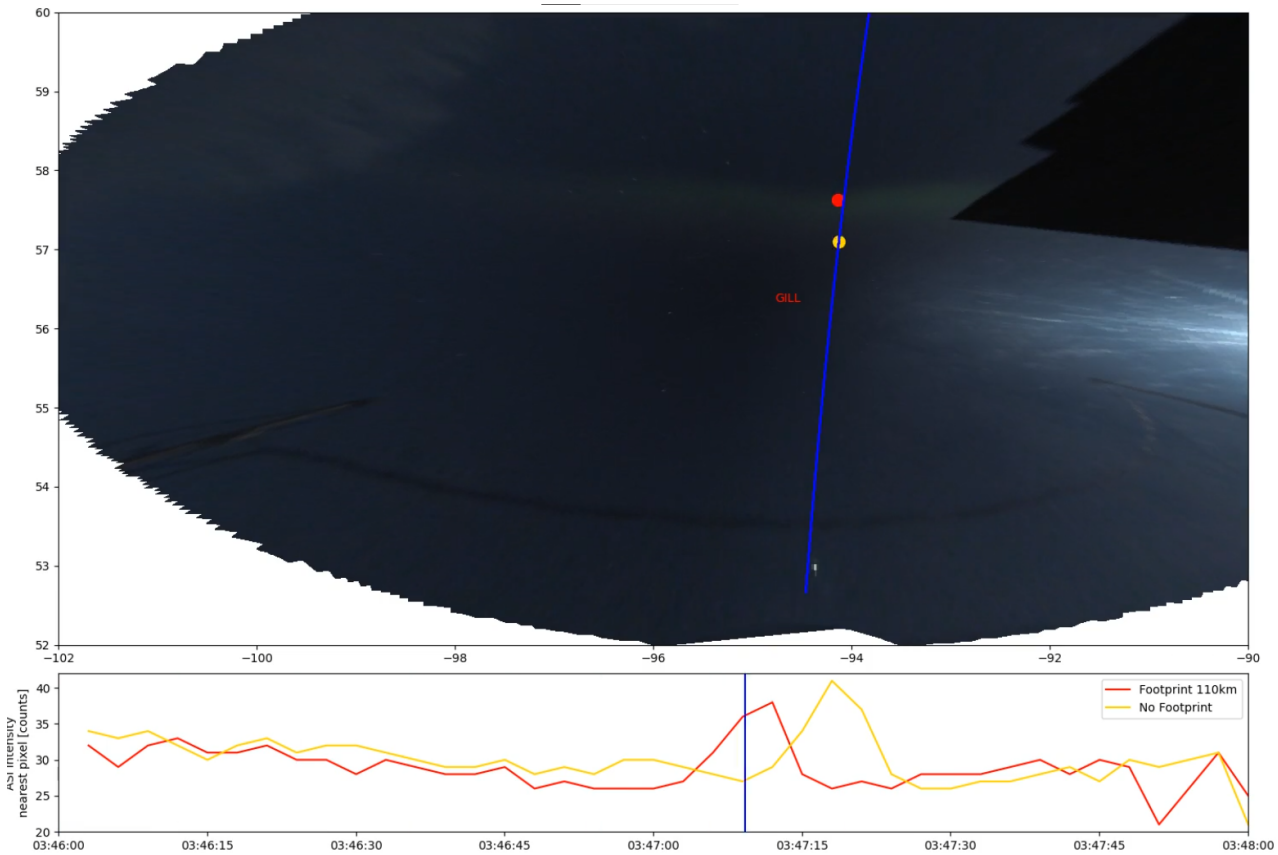

Figure 4: Footprint of GILL all sky camera with the TREx-RGB camera mapped to 110km. The red dot is the foot printed value and the yellow is the non-foot printed latitude. Note there is some longitudinal variations between the two. This is due to the fact that the dipole field is not mapped to the geographic mapping where our images are.

5 Toy Model Testing With Non-stationary Signals

Alfven-waves from the ionosphere are time-dependent waves so we can not assume they are stationary. Additionally, the perturbations measured by the Electric Field Instrument [20] in Swarm are under sampled for the time-scale we are interested in so we want to A: Construct a time series with time-dependent waves and B: Have properly sampled data in 50Hz Magnetic Field Instrument to be down sampled to be under sampled at 16Hz. [7] We construct three four second signals of approximately 1Hz, 2.5Hz and a chirp that goes from 2-9Hz. We then look at how we can best look at the data such that we recover as much information when down sampling the sampling rate from 50Hz to 16Hz. Its important to note that the 9Hz chirp will not be able to be captured in the 16Hz down sample because of the Nyquist frequency; however, this is realistic example as Alfven waves can have frequencies from 1-10Hz. [7].

To down sample, we looked at two different interpolation schemes, Fourier interpolation and sinc interpolation.

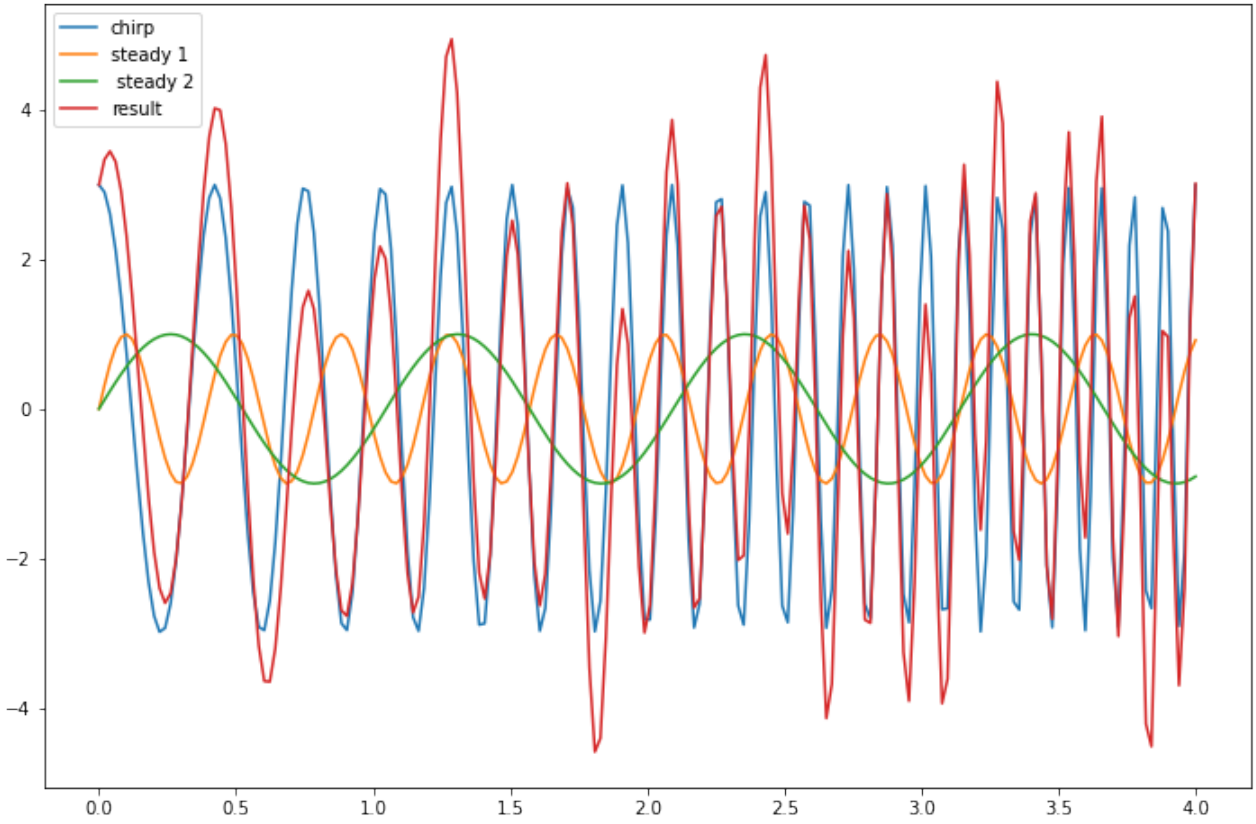

Figure 5: Three sine waves and the product of the three sin waves together with a sampling rate of 50Hz. The green is 1Hz, orange 2.5Hz, blue is a chirp from 2-9Hz (outside Nyquist frequency of 16Hz), the red is the superposition of the sine and chirp waves.

5.1 Resampling Methods

Looking at two resampling methods, first we tested the Shannon-Whitaker sinc interpolation method. [21] The Shannon-Whitaker sinc interpolation method is extremely powerful it will give a mathematically ideal band-limited replication of the signal (see sampling theorem)[22] The Shannon uses sinc waves to interpolate data using the following scheme

$$x(t) = \sum_{n=-\infty}^{\infty} x_n \operatorname{sinc}\left(\frac{t - nT}{T}\right)$$

where t is time, and T is sampling period, or $T = \frac{1}{f_s}$. The physical interpretation of this method is that it is using a infinite (or a very large sum for numerical analysis) superposition of sinc functions to re-create the original function with whatever time delimitation is asked (in our case 16Hz). In practice, the number of superposition's used is the same as your sampling frequency. This leads to interpolation errors as the number of sinc functions used needs to be infinite to be perfectly accurate;

however, a larger source of error are frequencies above the Nyquist which can not be resolved by sinc interpolation and instead to aliasing as seen in figure 6.

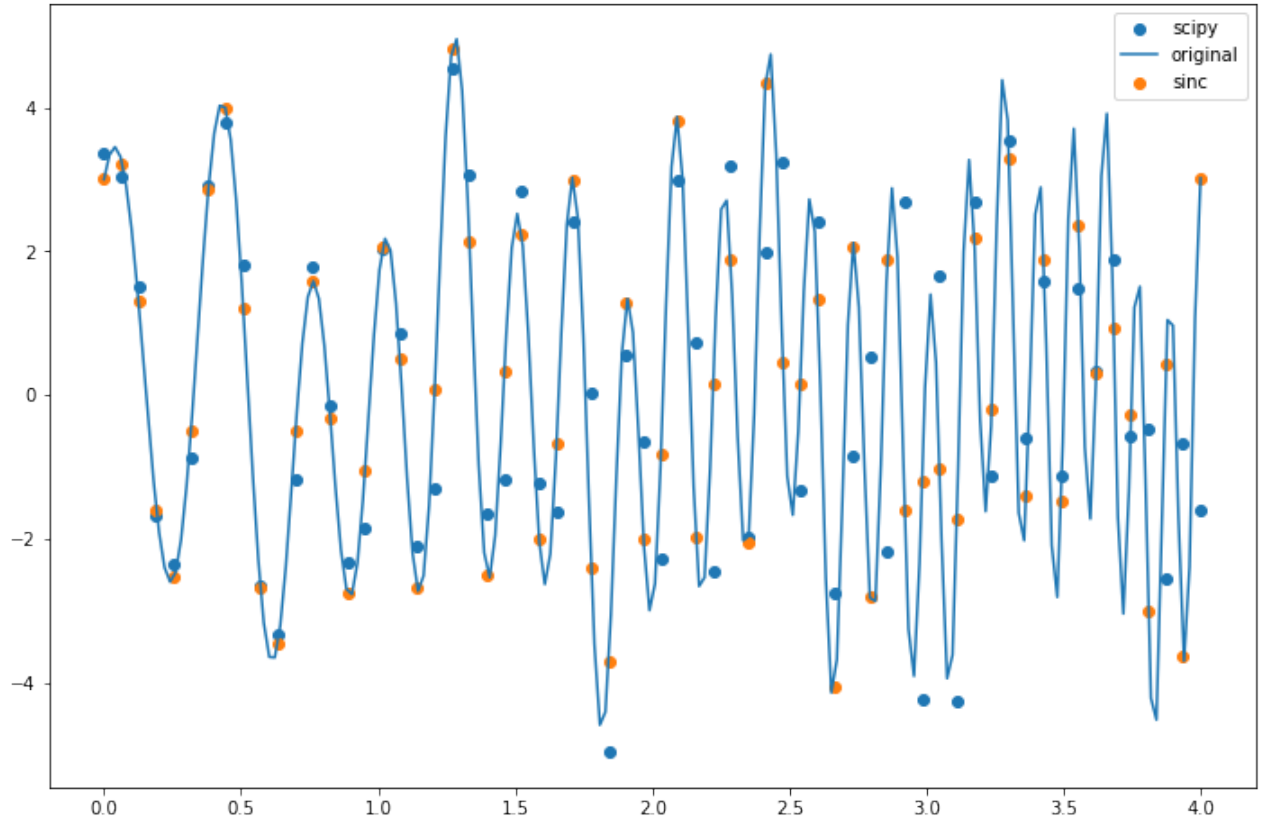

Figure 6: Non band passed interpolation of the sine waves and chirp. Both interpolation methods suffer from aliasing and from undersampling in the high frequency regime. This is a realistic example of the frequencies seen on Swarm so investigate filters is important.

Additionally, scipy's [23] implementation of a Fourier resampling method was tested. This assumes the signal is periodic which is not generally a suitable condition in the ionosphere where Alfven waves are present. The algorithm itself transforms the signal into the frequency domain, then it downsamples in the frequency space using sinc interpolation. The downsampled frequency domain signal is then turned back into the time domain. [23] However, the advantage of this method is that is down samples through the frequency domain, meaning that the signal will be an down sampling first and foremost in the frequency space. A result of this is the frequency response of the signal is prioritized over the time-domain. Due to do the time-dependent nature of the chirp, which clearly violates stationary (periodic) condition, a phase change is introduced in the time-domain. If this is present in the $\vec{B}$ data in our "real" analysis, then a Fourier method will be invalid.

5.2 Filter and Toy Results

Since we are interested in the $\frac{E}{B}$ ratio, its important to preserve where the sampling is located, rather than the signal produced by the Fourier transform. As seen in figure 6, Fourier resampling method does not do a good job and the sinc interpolation suffers from aliasing. To find this we can use

a low-pass filter. We use a low-pass butter worth filter of order 15 with a cutoff value of 7.5Hz. Doing this one time however reveals a phase offset and the lack of data near the beginning. This is because the butter worth filter is phasic and we need to go forward and backwards in the filtering. This doubles the band attentunation in exchange for fixing the delay. With our band-passed data we

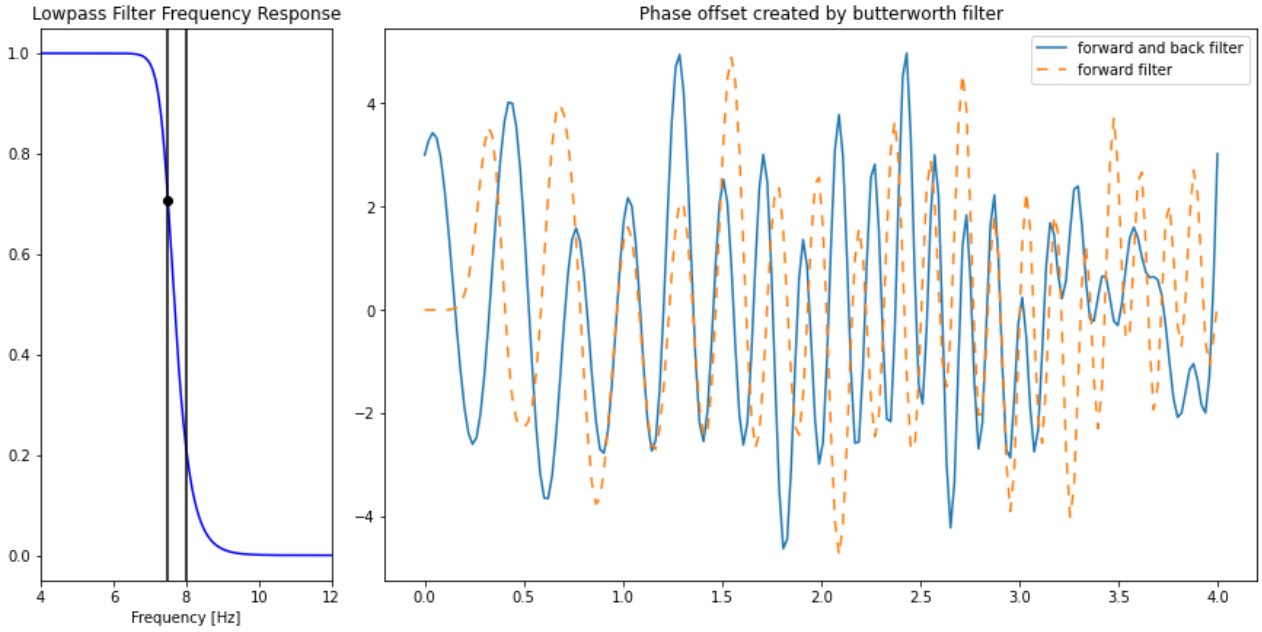

Figure 7: Butter worth filter and its frequency response (left). The difference between the half and full filtering scheme using the butter worth filter. Note the phase difference due to the effects of forward filtering rather than going forward and then back.

can now know that our sinc interpolation will perform well in the frequency regime prescribed. Any errors are associated with the number of sinc functions used in the superposition. As we can see in figure 7, the fit produced by the sinc function performs well but does miss a few peaks.

Moreover, the Fourier method does perform well when the signal is mostly stationary, but as the higher frequency chirp commences, a phase difference is introduced. This is indicative that the interpolation scheme is struggling as its assumptions are not holding. Unlike the sinc interpolation the amplitude is well preserved which is important when looking at the amplitude spectra in the next section.

5.3 Fourier Transforming data

Now lets take a Fourier transform of our data. We will be using periodograms. Since python is used, we are using scipy's periodogram function [23]. Periodograms differ from Fourier transforms as they take the power spectrum of the signal. This is done by splitting up our window into different mini windows. Each mini window has its fourier transform taken then combined together. For scipy's implementation this is at maximum 8 windows. This periodogram function calls an N (array size) length Hann window, 0 overlap Welch function. [23] [24] Zero overlap Welch functions are also known as Bartlett's methods. The advantage to having no overlap is that it minimizes the effects of having outlier data as if you had an outlier, it would show up in multiple windows, exacerbating

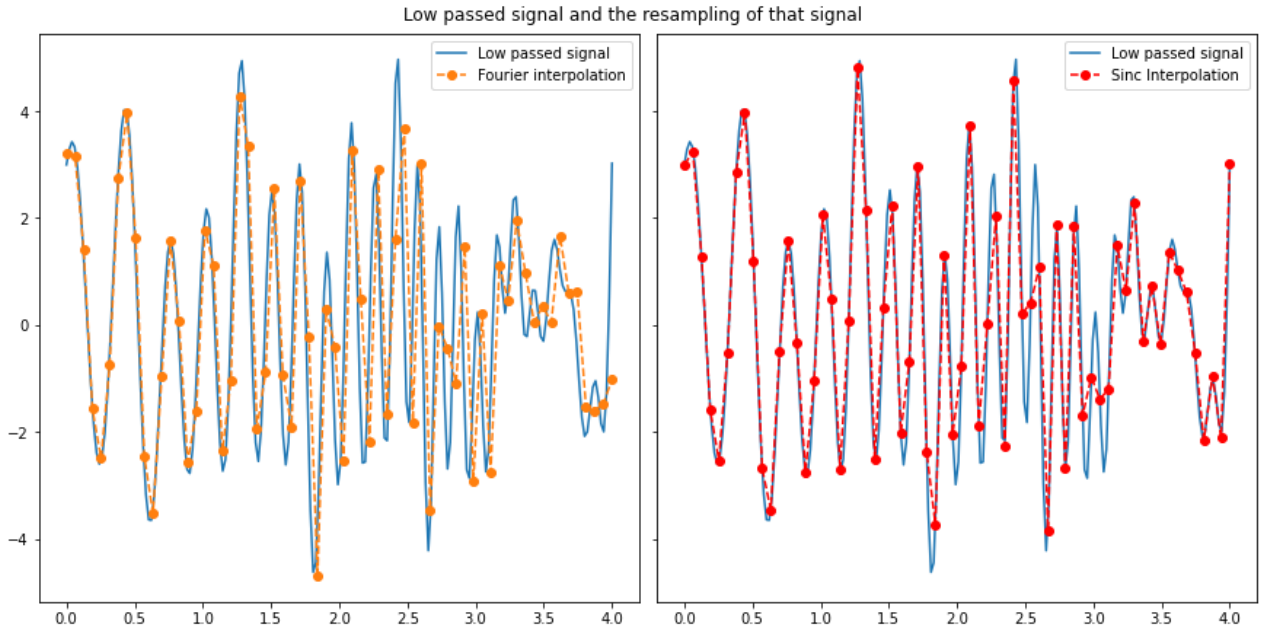

Figure 8: Over plots of the low passed 50Hz signal over the interpolation schemes of 50Hz to 16Hz. Generally both plots perform well in the stationary phase. When aliasing occurs due to a lack of sampling in the sinc interpolation, it fails to capture the data whereas in the Fourier interpolation, a phase offset is introduced why the relatively amplitudes are kept the same.

the effect. [25] The data provided by Swarm does not have error bars for each data point but rather clumps it up in large sections so its safer to assume that there are significant variations. A downside to this approach is the sampling rate of the periodogram in frequency space is reduced. Additionally, we also apply a linear detrend, although not needed in the case of our sine waves (oscillates around 0), the auroral oval has stationary field aligned currents which (by themselves) do not oscillate on Alfvenic time scales but do have linear signals. [7]

As seen in figure 8, our frequencies around 7.5Hz are being removed which is intended. Additionally, during the chirp, the sampling is slightly different between 50Hz and 16Hz in the frequency space so some resolution is lost particularly in the 5-7Hz region. Arguments can be made as to whether this is okay as our Alfven waves will be present, and mostly likely obvious, in these frequency bands; however, I think its is acceptable result. If we wanted to increase our sampling rate to better replicate the data, we could introduce more overlap. as well as the Fourier interpolation working wonders as replicating the data as it is doing the sinc interpolation in the frequency space to begin with. We see a perfect replication of the low passed 50Hz signal; however, its clear that the sinc interpolation struggles here. This is because of the order of operations we are performing. Sinc interpolation should be used when we are working in the time domain whereas the Fourier interpolation should be used when working in the frequency domain.

6 Replicating Miles et. al paper

In Miles et al. 2018, a close conjunction was found between e-pop and Swarm A and C. The imager on the e-pop probe was active and captured the aurora two minutes after the Swarm satellites passed.

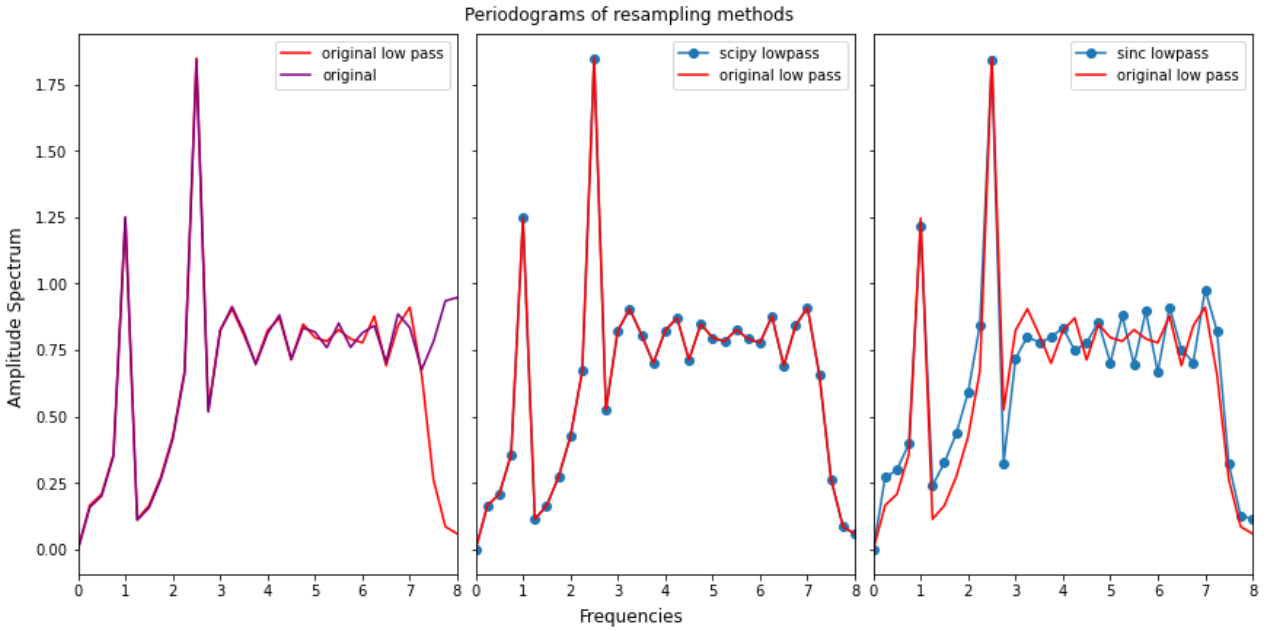

Figure 9: Original signal versus the low pass signal at 50 hertz using the periodogram method(a), periodogram of the Fourier Interpolation scheme for 50Hz to 16Hz in the frequency domain over plotted with the low-passed signal periodogram (middle), periodogram of the sinc interpolation over plotted with the low-passed signal periodogram (right)

By inferring the position, it was found that there was a correlation between perturbations in the electric and magnetic field components during the event and the presumed auroral signature.

6.1 Data Processing

The quality of the electric field instrument during this time is good; however, there are transients which cause large spikes. Additionally, the method for fitting the velocities in $\vec{E} = \vec{v} \times \vec{B}$ has changed between data releases from when the original paper was published. As described earlier, the Electric field instrument collects the velocities using histograms, the fit of these histograms are the difference in these data releases. The magnetic field data has not changed as is preserved in the 50Hz cadence (though there are slight differences in the 16Hz as a cubic spline is used alongside the band pass filtering which affects the spline fit of the 50Hz).

6.1.1 Electric field data

To address the spikes in figure 11, we use a 20 second running average. If these values are 15x the value of the running average, they are moved and then interpreted with a sinc function. In Miles et al.'s paper, a spline interpolation is used instead of the sinc interpolation. As seen in the bottom panel of figure 11, the are slight differences that are not entirely explainable by the fit scheme (as there are only a few transients). Instead these are due to the new data releases. The periodograms that result from the new data releases and the old data releases will be slightly different but it should still be a sufficient quality check.

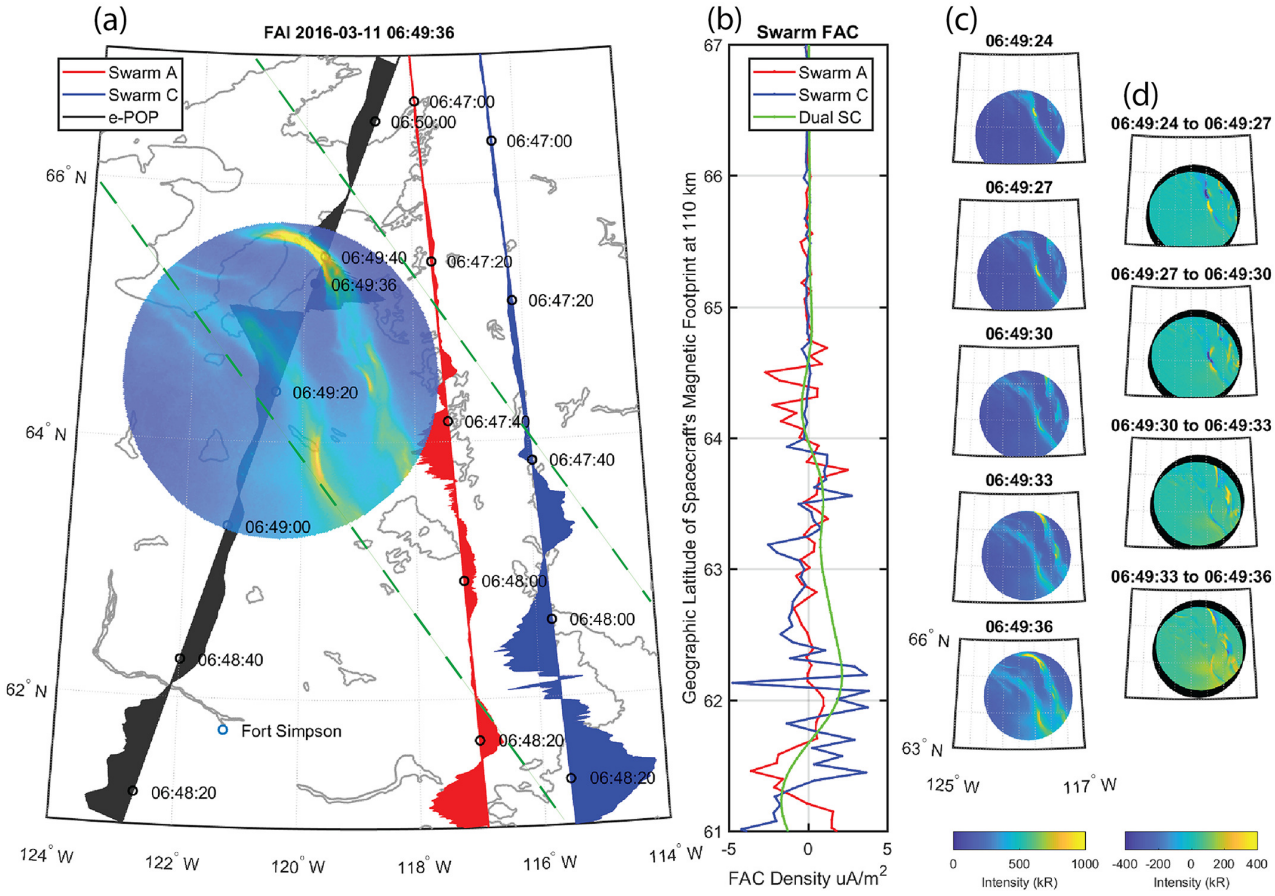

Figure 10: Mapped, near conjugate measurements from e-POP (black) and Swarm A (red) and C (blue) spacecraft. (a) Spacecraft tracks overlaid on a coastline map; the dashed green lines extrapolate the general region of the arc, FAI near-infrared image from 06:49:36 UT, with superposed cross-track magnetic perturbations. (b) Field-aligned current density as estimated by single spacecraft methods for Swarm A (red), Swarm C (blue), and by the Swarm dual spacecraft integral method (green). (c) e-POP FAI images at 3 s intervals showing dynamic aurora. (d) Differenced FAI images showing equatorward and poleward motions of southern and northern arc features, respectively. See text for details. [7]

6.2 Periodograms

Now taking a small period in which both auroral arcs are presumed to reside, we take the periodogram of E and B using the method in 5.3 to understand where our analysis has and hasn't worked.

First its important to note, looking at figure 11 and figure 12, the time period in which the arcs are characterized by optical signature are corresponding to multiple transients, so the interpolation method will be exacerbated here as compared to other regions of the time series. Additionally, looking at the electric field during this time period in figure 12, it seems like when the resonator is most active (that is there are large oscillations of over 5mV), it has been smoothed out in the new data release, however the signature is still present. As a result the amplitude spectra for the electric fields are quite different.

Moreover, investigate the magnetic and the resampling. We can see the sinc interpolation gives

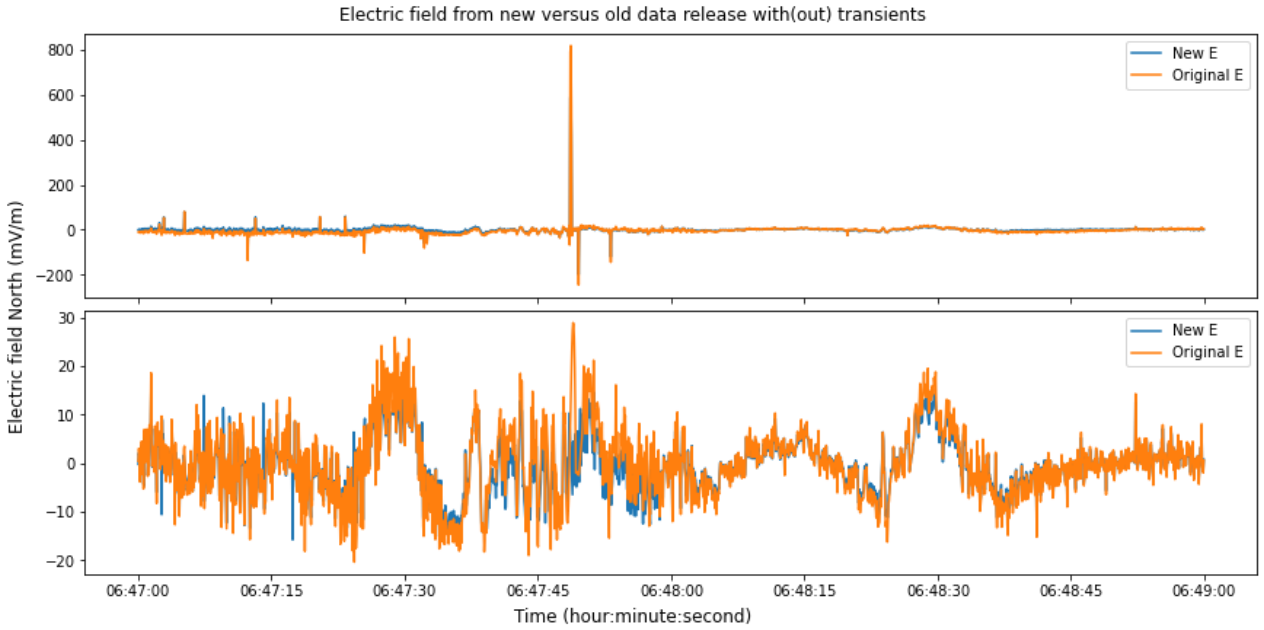

Figure 11: Transients in the data. Note the new data releases also have them, but they are lower magnitude and are obscured by the higher amplitude ones of the old data set (bottom). Below is the Electric field with the new and old release. Note the differences are slightly obscured by the different interpolation schemes for the transients but these are negligible compared to the different processing technique

the exact same periodogram of the spline interpolation of Miles et al.'s data. This makes sense as most interpolation methods use spline interpolation as its much less computationally expensive as the sinc function while still achieving a good result. Even more interesting however is the Fourier interpolation versus spline interpolation. While the low frequency regime are near identical (stationary condition is true), approaching and passing 3Hz, there starts to be discrepancies between the interpolation schemes. As discussed in 5.3, this is because the resampling method is first taking the Fourier transform then down sampling that which leads to a more "accurate" result in frequency space, but a phase offset and aliasing in the time domain. For this reason the Fourier interpolation is actually doing better at resampling since we are only interested in the frequency domain for this analysis.

7 Synthesis of In-situ Measurements

Sections of B which are characterised by large dB for a window of around 2-5 seconds are known as field aligned currents. These are the currents which carry ions and electrons from the plasma sheet to the ionosphere. Fluctuations in these large scale currents are investigate to be Alfven waves. Its important to note that the spatial scale of the IAR should be producing small-scale dynamics on the order of 1-10km.[7] This corresponds to the small wiggles embedded in the field aligned currents.

Dividing an auroral crossing into sections there are field aligned current downward, in which electrons go upwards, the dark aurora where there is no current but the electric and magnetic fields are disturbed but there is Little dB or dE, and the visible aurora (upward field aligned current)

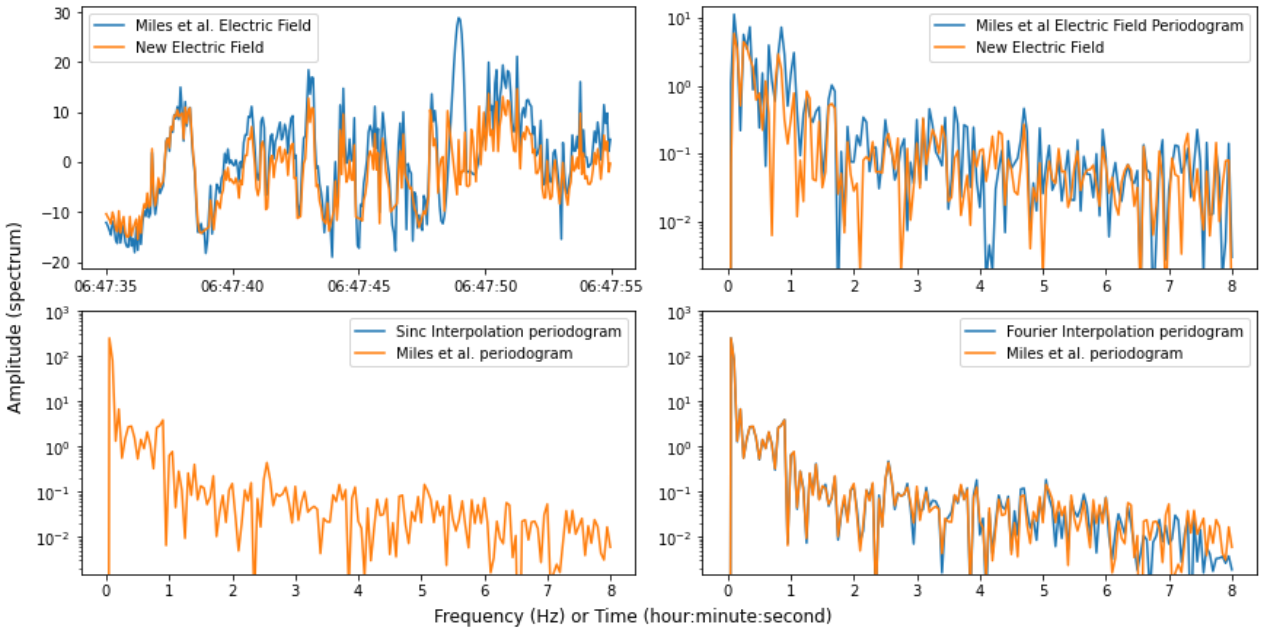

Figure 12: Top left: Pop out of Electric field from Miles et al. versus the new processing, Top right: Periodograms of the Electric field, Bottom left: Periodogram of the sinc interpolation versus the spline interpolation from previous, Bottom right: Fourier interpolation versus spline interpolation

which is caused by electrons participating down into the ionosphere. Wu et al. 2020 found that the location of Alfven waves is dependent on the structure and time of the Aurora activity [26]. This was a statistical survey but it would be beneficial to understand the location of the Alfven waves in relation to the large scale auroral structures. It also a natural progression of the Mile's et al.'s paper as that considered the periodogram, conductivity, and Alfven speed over the auroral pass rather than delimiting between field aligned regions.

As described in section 4, a close conjunction occurred with a single discrete arc at 03:46-03:48UTC. The electric and magnetic fields instruments were running and when correlated with optical measurements an upward field aligned current (electrons downward) co-aligned with optical measurements as expected. No wave signatures were present in the upward current; however, due to the local dependence found by Wu, we found Alfven signatures in the downward current and dark auroral (between two current) regions. See Supporting Video for the animation correlating Optical measurements, location, and Magnetic and Electric fields during the auroral pass.

Figure 13 shows the Magnetic, Electric fields, their derivatives (to visually find oscillations), the periodogram of E and B and their ratio and the optical emission at the location of the satellite. The method to find all the above is described in the respective sections. As seen in the 2nd column, the electric field instrument is inherently nosier the well behaved magnetic field instrument. However, there is are sections visually where the dB and dE are either in phase or anti-phase. When the derivatives are in phase it means that there could be an Alfven wave at that location. This is generally quite messy however and the wave-nature of the IAR is much clearer in the peridogram as expected. Particularly in periodogram of B, there are clear harmonics and nodes showing the resonator is active during this 5 second segment sampled. Again the E is largely unclear but particularly at the 4Hz mark, you can see the E and B periodogram's line up and in the E/B ratio, there is a corresponding

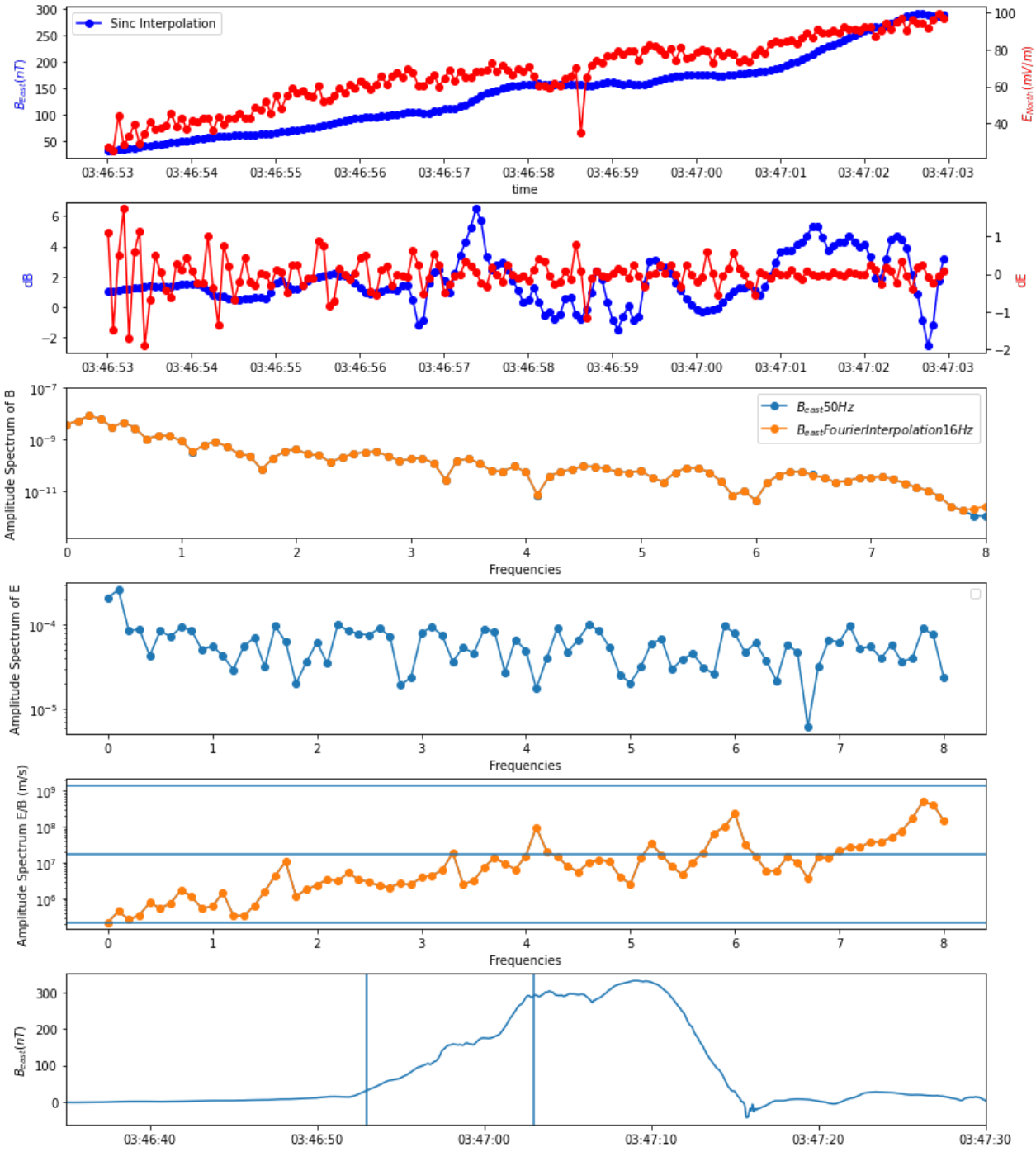

Figure 13: Synthesis of toy model using real data. 1: twin axis with relevant E and B components, 2: twin axis with relevant dE and dB components, Amplitude spectra of B, Amplitude spectra of E, Amplitude Spectra of E/B where the bottom horizontal line is the theoretically minima, the middle horizontal line is the Alfven speed, V_A, and the top horizontal line is the theoretically maxima $V_A^2 \Sigma \mu_0$, and a B component with vertical lines denoting the time range used for the ratio

maxima in the resonating cavity. Taking the zeroth order frequency, and using the formula [5]

$$\frac{E_{pe}}{B_{pe}} = \frac{1}{\Sigma \mu_0} \tag{1}$$

we find a conductivity in this region of $\Sigma = 3.58S$ and a Alfven speed (mean value) of $V_A = 1778$km/s. These are both believable values, however the mean value as an oscillation point is quite vague given the data so its quite possible that there are significant errors.

Moving onto the dark region from 3:47:02 to 3:47:11, we find a conductivity of $\Sigma = 8.02S$ and an Alfven speed of $V_A = 2748$km/s. During the upward field aligned current however, as there is no oscillations our periodogram is effectively flat when detrended, giving a conductivity of $\Sigma = 0.94$ and an Alfven speed of $V_A = 860$km/s. As discussed in 3.2, because the sigma is close and below zero, we can not believe our sigma estimation.

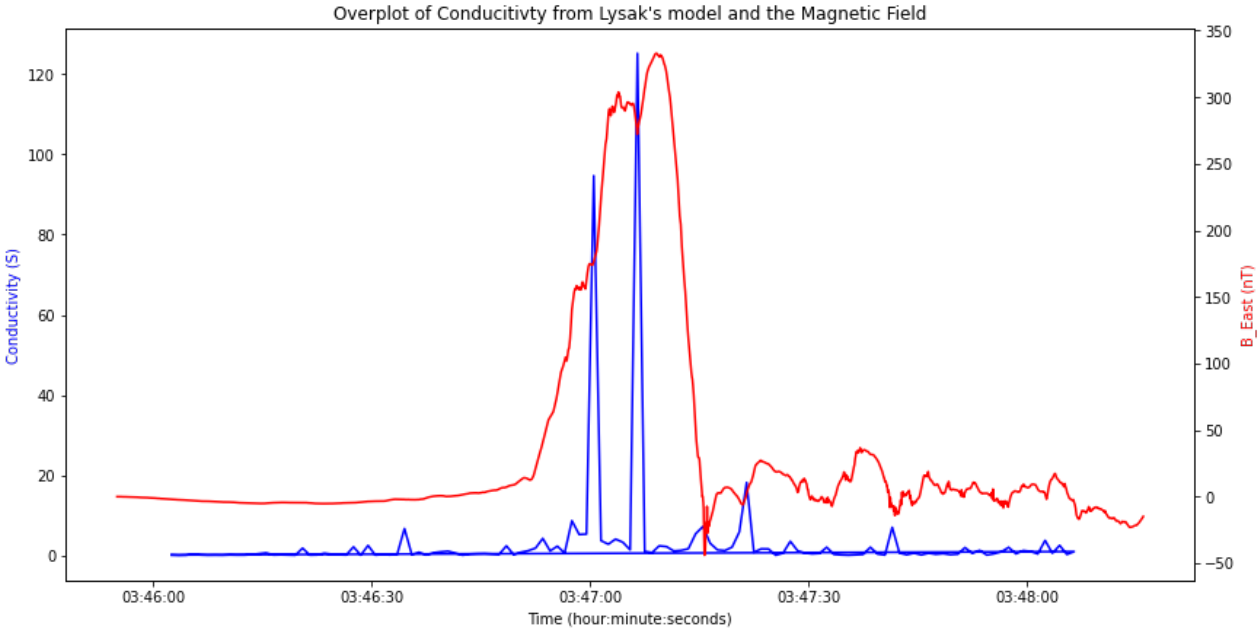

Figure 14: Over plot of Magnetic field (red) and the conductivity predicted by the zeroth frequency estimate. Increases of conductance are (visually) correlated with oscillations in B.

An analysis was also done using a 5 second running average with one second increments. Using an N length Hanning window as described in 5.3, the Hanning window selects the middle $\pm 1.5 seconds$ and then the other second on either side is used to drown out noise. [11] With this scheme we can get self-consistent results but also find the changes in Conductivity through the satellite track with a very fine degradation. Taking the mean value of the time in thewindow and finding the associated conductivity of that window, we constructed a time series of the conductivity through time along the track.

Inspecting the results of the running window analysis, we generally see that increases in the conductivity of the ionosphere is correlated with wiggles in B. Throughout the downward field aligned current we see an increase in the conductivity. Then this conductivity disappear as the model starts to fail in the upward field aligned current. What is more interesting is the conductivity generally spikes (sometimes radically so) when there are wiggles in B both in the downward field aligned current and the first section of the dark aurora. Where these wiggles are, there is more signal to noise for the periodogram to pick out so our values of conductivity should be better and it would make sense for the conductivity to increase where the resonating is active as it means Alfven waves are present and are transmitting current (increasing conductivity).

To better explain the two spikes (which predict a conductivity 10x to 100x greater than predicted), we could decrease the step in which the running window goes through. By varying by 0.25 seconds we could smooth out these spikes. As of right now I would not trust the values predicted by the spikes; however, the general trend of oscillations in B corresponding to a increase of conductivity confirms that when Resonator is active, Alfven waves are modulated and areas where more Alfven waves are measured correspond to more current measured.

8 Future Works

Future works analysis of the Alfven speed through the auroral oval. Additionally, understanding where Alfven waves are located in multi-arc systems is extremely interesting as there are multiple field aligned currents integrated into the system. Additionally, other analysis of the conductivity, using simpler estimations are available and should be compared to see where traditional model (or Alfven models) fail to capture the conductivity in the ionosphere.

Additionally, we could implement a Bayesian Monte Carlo network to try to fit our data E/B ratio to the reflection ratio predicted by Lysak's model. This fitting would tell us how well the model and its parameters fit the data, giving an error for the conductivity and Alfven speed, and also could tell us if there are multiple different resonators active within one pass (would give a multi-variant Gaussian). Work on fitting the model to model using Bayesian probability was done during spring break; however, due to time constrains and testing on the model not being completed, it did not progress past some initial testing.

9 Acknowledgements

First I want to thank Ian Mann for taking me on as a supervisor. His continued support throughout difficult sociopolitical situations can not be understated. Additionally, his willingness to let me learn and make mistakes and trust that it will result in thought provoking quality research has been greatly appreciated. His attention to detail keeps me diligent and produced a quality of research of the highest quality and I look forward to our continued work in the future.

Second I want to thank Abby Azari for coming on-board to discuss Monte Carlo simulations which were the focus for a few weeks but could not effectively be conducted as the data quality was not sufficiently rigorous yet. I look forward to working with them in the future and I hope during the summer or on the side this project can be generalized using their statistical skill set. Additionally, on a more personal note, I appreciate their ability to be honest and guide me through logic that can be difficult to discuss during meetings (especially during DASP). These allowed me to foundationalize my thought processes as a early-career scientist.

I also want to thank Patrick Hall from York University and Edwin Genoud-Prachex from Goethe University for taking me on a student last winter and introducing me to quasar cosmology and more important Bayesian Monte Carlo methods which have been invaluable to my progress as a scientist and have formed my approach to research I want to conduct

Lastly I want to thank Richard Sydora for introducing me to research and most importantly Alfven waves! I have learned so much during and after that first research term and I am thankful to him for agreeing to liaison this project while Dr. Mann is away.

References

[1] F.F. Chen. *Introduction to Plasma Physics and Controlled Fusion*. Number v. 1 in Introduction to Plasma Physics and Controlled Fusion. Springer, 1984.

[2] Manfred Scholer. On the motion of artificial ion clouds in the magnetosphere. *Planetary and Space Science*, 18(7):977–1004, 1970.

[3] IR Mann, DK Milling, IJ Rae, LG Ozeke, A Kale, ZC Kale, KR Murphy, A Parent, M Usanova, DM Pahud, et al. The upgraded carisma magnetometer array in the themis era. *Space Science Reviews*, 141:413–451, 2008.

[4] Robert L. Lysak. Feedback instability of the ionospheric resonant cavity. *Journal of Geophysical Research: Space Physics*, 96(A2):1553–1568, 1991.

[5] M. Ishii, M. Sugiura, T. Iyemori, and J. A. Slavin. Correlation between magnetic and electric field perturbations in the field-aligned current regions deduced from de 2 observations. *Journal of Geophysical Research: Space Physics*, 97(A9):13877–13887, 1992.

[6] DJ Knudsen, MC Kelley, GD Earle, JF Vickrey, and M Boehm. Distinguishing alfvén waves from quasi-static field structures associated with the discrete aurora: Sounding rocket and hilat satellite measurements. *Geophysical Research Letters*, 17(7):921–924, 1990.

[7] D. M. Miles, I. R. Mann, I. P. Pakhotin, J. K. Burchill, A. D. Howarth, D. J. Knudsen, R. L. Lysak, D. D. Wallis, L. L. Cogger, and A. W. Yau. Alfvénic dynamics and fine structuring of discrete auroral arcs: Swarm and e-pop observations. *Geophysical Research Letters*, 45(2):545–555, 2018.

[8] Dieter Bilitza, David Altadill, Yongliang Zhang, Chris Mertens, Vladimir Truhlik, Phil Richards, Lee-Anne McKinnell, and Bodo Reinisch. The international reference ionosphere 2012–a model of international collaboration. *Journal of Space Weather and Space Climate*, 4:A07, 2014.

[9] J. W. Gjerloev and R. A. Hoffman. Height-integrated conductivity in auroral substorms: 2. modeling. *Journal of Geophysical Research: Space Physics*, 105(A1):227–235, 2000.

[10] Abril-Pla Oriol, Andreani Virgile, Carroll Colin, Dong Larry, Fonnesbeck Christopher J., Kochurov Maxim, Kumar Ravin, Lao Jupeng, Luhmann Christian C., Martin Osvaldo A., Osthege Michael, Vieira Ricardo, Wiecki Thomas, and Zinkov Robert. Pymc: A modern and comprehensive probabilistic programming framework in python. *PeerJ Computer Science*, 9:e1516, 2023.

[11] E. Friis-Christensen, H. Lühr, D. Knudsen, and R. Haagmans. Swarm – an earth observation mission investigating geospace. *Advances in Space Research*, 41(1):210–216, 2008.

[12] D. J. Knudsen, J. K. Burchill, S. C. Buchert, A. I. Eriksson, R. Gill, J.-E. Wahlund, L. Åhlen, M. Smith, and B. Moffat. Thermal ion imagers and langmuir probes in the swarm electric field instruments. *Journal of Geophysical Research: Space Physics*, 122(2):2655–2673, 2017.

[13] Jos é M. G. Merayo, John L. Jørgensen, Eigil Friis-Christensen, Peter Brauer, Fritz Primdahl, Peter S. Jørgensen, Thomas H. Allin, and Troelz Denver. *The Swarm Magnetometry Package*, pages 143–151. Springer Netherlands, Dordrecht, 2008.

[14] Johnathan K Burchill and David J Knudsen. Swarm thermal ion imager measurement performance. *Earth, Planets and Space*, 74(1):181, 2022.

[15] Christopher C. Finlay, Nils Olsen, Stavros Kotsiaros, Nicolas Gillet, and Lars Tøffner-Clausen. Recent geomagnetic secular variation from Swarm and ground observatories as estimated in the CHAOS-6 geomagnetic field model. *Earth, Planets and Space*, 68(1):112, July 2016.

[16] M. Shumko, D. Chaddock, B. Gallardo-Lacourt, E. Donovan, E. L. Spanswick, A. J. Halford, I. Thompson, and K. R. Murphy. Aurorax, pyaurorax, and aurora-asi-lib: A user-friendly auroral all-sky imager analysis framework. *Frontiers in Astronomy and Space Sciences*, 9, 2022.

[17] D. M. Gillies, J. Liang, E. Donovan, and E. Spanswick. The apparent motion of steve and the picket fence phenomena. *Geophysical Research Letters*, 47(20):e2020GL088980, 2020. e2020GL088980 2020GL088980.

[18] Daniel Boscher, Sebastien Bourdarie, Paul O'Brien, Tim Guild, Daniel Heynderickx, Steve Morley, Adam Kellerman, Christopher Roth, Hugh Evans, Antoine Brunet, Mykhaylo Shumko, Colby Lemon, Seth Claudepierre, Thomas Nilsson, Erwin De Donder, Reiner Friedel, Stu Huston, Kyungguk Min, Alexander Drozdov, and IRBEM Contributor Community. Prbem/irbem: v5.0.0, July 2022.

[19] S. G. Shepherd. Altitude-adjusted corrected geomagnetic coordinates: Definition and functional approximations. *Journal of Geophysical Research: Space Physics*, 119(9):7501–7521, 2014.

[20] D. J. Knudsen, J. K. Burchill, S. C. Buchert, A. I. Eriksson, R. Gill, J.-E. Wahlund, L. Åhlen, M. Smith, and B. Moffat. Thermal ion imagers and langmuir probes in the swarm electric field instruments. *Journal of Geophysical Research: Space Physics*, 122(2):2655–2673, 2017.

[21] Alan V. Oppenheim. Digital signal processing / [by] alan v. oppenheim [and] ronald w. schafer., 1975.

[22] Wikipedia contributors. Whittaker–shannon interpolation formula — Wikipedia, the free encyclopedia, 2023. [Online; accessed 29-February-2024].

[23] Pauli Virtanen, Ralf Gommers, Travis E. Oliphant, Matt Haberland, Tyler Reddy, David Cournapeau, Evgeni Burovski, Pearu Peterson, Warren Weckesser, Jonathan Bright, Stéfan J. van der Walt, Matthew Brett, Joshua Wilson, K. Jarrod Millman, Nikolay Mayorov, Andrew R. J. Nelson, Eric Jones, Robert Kern, Eric Larson, C J Carey, İlhan Polat, Yu Feng, Eric W. Moore, Jake VanderPlas, Denis Laxalde, Josef Perktold, Robert Cimrman, Ian Henriksen, E. A. Quintero, Charles R. Harris, Anne M. Archibald, Antônio H. Ribeiro, Fabian Pedregosa, Paul van Mulbregt, and SciPy 1.0 Contributors. SciPy 1.0: Fundamental Algorithms for Scientific Computing in Python. *Nature Methods*, 17:261–272, 2020.

[24] P. Welch. The use of fast fourier transform for the estimation of power spectra: A method based on time averaging over short, modified periodograms. *IEEE Transactions on Audio and Electroacoustics*, 15(2):70–73, 1967.

[25] M.H. Hayes. *Statistical Digital Signal Processing and Modeling*. Wiley, 1996.

[26] J. Wu, D. J. Knudsen, D. M. Gillies, and J. K. Burchill. Swarm survey of alfvénic fluctuations and their relation to nightside field-aligned current and auroral arc systems. *Journal of Geophysical Research: Space Physics*, 125(3):e2019JA027220, 2020. e2019JA027220 10.1029/2019JA027220.